3D thermoplastic elastomer microfluidic devices for biological probe immobilization

Brassard, Daniel; Clime, Liviu; Li, Kebin; Geissler, Matthias; Miville-Godin, Caroline; Roy, Emmanuel; Veres, Teodor

Publisher's version / Version de l'éditeur:
https://doi.org/10.1039/C1LC20714H
Lab on a Chip, 11, 23, pp. 4099-4107, 2011-10-31

PAPER www.rsc.org/loc | Lab on a Chip

3D thermoplastic elastomer microfluidic devices for biological probe immobilization

Daniel Brassard,* Liviu Clime, Kebin Li, Matthias Geissler, Caroline Miville-Godin, Emmanuel Roy and Teodor Veres

Received (in XXX, XXX) Xth XXXXXXXXX 2011, Accepted Xth XXXXXXXXX 2011
First published on the web Xth XXXXXXXXX 2011
DOI: 10.1039/b000000x

Microfluidics has emerged as a valuable tool for the high-resolution patterning of biological probes on solid supports. Yet, its widespread adoption as a universal biological immobilization tool is still limited by several technical challenges, particularly for the patterning of isolated spots using three-dimensional (3D) channel networks. A key limitation arises from the difficulties to adapt the techniques and materials typically used in prototyping to low-cost mass-production. In this paper, we present the fabrication of thin thermoplastic elastomer membranes with microscopic through-holes using a hot-embossing process that is compatible with high-throughput manufacturing. The membranes provide the basis for the fabrication of highly integrated 3D microfluidic devices with a footprint of only 1 × 1 cm^2. When placed on a solid support, the device allows for the immobilization of up to 96 different probes in the form of a 10 × 10 array comprising isolated spots of 50 × 50 μm^2. The design of the channel network is optimized using 3D simulations based on the Lattice-Boltzmann method to promote capillary action as the sole force distributing the liquid in the device. Finally, we demonstrate the patterning of DNA and protein arrays on hard thermoplastic substrates yielding spots of excellent definition that prove to be highly specific in subsequent hybridization experiments.

1. Introduction

The immobilization and patterning of biological probes on solid supports is central to numerous biological assays.[1,2] DNA and protein microarrays, for example, offer the possibility to study concurrently the interaction between a target sample and a large number of probes, which makes them indispensible for many areas including drug discovery,[3,4] clinical diagnostic,[3,5] and gene sequencing.[6,7] However, microarrays still largely depend on detection techniques such as fluorescence labeling or surface plasmon resonance which are difficult to apply to point-of-care applications. Recently, new detection techniques involving arrays of integrated sensors with microfabricated biosensing elements have emerged,[8] including: nanowires,[9-12] field-effect-transistors,[13,14] optical waveguides,[15-19] and electrochemical sensors.[20] This new generation of microfabricated biosensor arrays creates a pressing need for the development of techniques that allow various biological probes to be immobilized with high positional accuracy on micron-size sensing elements.

The immobilization of DNA, proteins, cells or other biological probes on a solid surface can be achieved by a number of techniques[1] including pin spotting,[21-23] inkjet printing,[24,25] microcontact printing,[3,26-28] and microfluidics.[18,19,29-49] Among these techniques, pin spotting has become the standard fabrication technology for DNA microarrays due to its relative simplicity and the possibility to produce a vast number of spots in an automated fashion.[1,22] Pin spotting employs a set of metallic micropins to deliver minute amounts of liquid upon contact with a surface. However, accurate positioning and registration of the spots between each successive printing cycle are difficult to control and require costly and sophisticated tools. Also, the rapid and uncontrolled drying of liquid can lead to non-uniform spots and denaturation of sensitive material, especially when the dimensions of the spots are decreased below ~80 μm.[1,22,23]

Microfluidics provides a simple and convenient path to control the immobilization conditions as well as the dimension, positioning, and uniformity of the deposited features.[18,19,29-47] To this end, microfluidic immobilization devices typically consist of a network of channels patterned in poly(dimethylsiloxane) (PDMS), a thermoset elastomer that can create reversible conformal sealing upon contact with a planar solid support. The network is filled with a solution comprising the biological probes followed by incubation and washing, which leads to an immobilized pattern matching the geometry of the channels. For example, line features with excellent uniformity spanning several centimeters in length and few micrometers in width have been achieved with this technique.[31,32] On the other hand, simple microfluidic devices having a 2D network of channels are inherently limited to pattern continuous features and cannot be used to form an array of isolated spots, as it would be required for the immobilization of biological probes only on the sensing

Industrial Materials Institute, National Research Council, 75 de Mortagne, Boucherville,QC, J4B 6Y4, Canada. E-mail: Daniel.Brassard@imi.cnrc-nrc.gc.ca; Tel: +1-450-641-5821

elements of a microfabricated biosensor array.[19]

To overcome this limitation, more complex designs based on a 3D channel configuration have been proposed. In these designs, the channels are typically embedded inside the microfluidic device and the liquid is brought in contact with the substrate only on the desired locations using open through-holes (i.e., "vias"),[36-41] channels oriented perpendicularly to the substrate,[42-46] or hydrodynamic flow confinement.[18,39,46] A 3D microfluidic immobilization device has first been demonstrated by Chui *et al*. using a thin PDMS membrane with open through-holes to make connections between two levels of channels.[36] Juncker *et al*. have also reported the fabrication of 3D microfluidic devices by etching open through-holes in silicon using deep reactive ion etching.[38-40] It is finally worth mentioning the recent work of Gale's and Myszaka's groups who designed a multilayer 3D patterning system based on channels oriented perpendicularly to the substrate allowing up to 48 independent biological probes to be immobilized on isolated spots that are ~400 μm in width and length.[42-46]

Despite these developments, many challenges must still be solved before microfluidics can be accepted as a universal biological patterning tool. The most critical issue arguably arises from the intrinsic need to use microfluidic devices only once to avoid cross-contamination issues, which demands for materials and techniques that promote high-throughput fabrication at low cost. However, almost all designs of microfluidic patterning devices have relied on PDMS,[18,19,31-37,40-49] which is not very amendable to low cost mass-production.[50-53] PDMS is also an hydrophobic material,[50] which favors the trapping of air bubbles in the channels and prevents the use of capillary action to fill the devices. Although the surface of PDMS can be made temporarily hydrophilic using O_2 plasma treatment, it will recover its hydrophobic state within few hours, which is problematic for 3D devices assembled from multiple layers.[31,50,54] Moreover, many of the 3D microfluidic designs proposed to date require the alignment of elastomeric layers over large areas in conjunction with costly and lengthy post-processing procedures to punch the numerous access holes and cut the devices to their final shape.[36,41-46]

Herein, we demonstrate a new fabrication technique for 3D microfluidic systems that can alleviate several of the shortcomings encountered in previous configurations. We have recently identified commercially available thermoplastic elastomers (TPE) that can adapt to other surfaces through conformal contact in a similar way than PDMS, while providing the appealing ability to be processed using conventional thermoforming methods such as hot embossing lithography (HEL) or injection molding.[29,53,55,56] In this paper, we extend this work by demonstrating the rapid and reliable patterning of open through-holes and channels in thin TPE membranes using a method based on HEL. We then discuss the design of a TPE-based 3D microfluidic patterning device that permits the immobilization of up to 96 different biological probes in a 10 × 10 array format of 50 × 50 μm^2 spots. We also present an optimization of the channel geometry using 3D Lattice-Boltzmann numerical simulations to ensure the complete filling of the devices using only capillary forces. We finally validate the performance of the device by immobilizing high-quality arrays of DNA and proteins on plastic substrates.

2. Design and fabrication

The microfluidic devices described in this paper were fabricated in Versaflex® CL30, a melt-processable styrene-ethylene/butylene-styrene block copolymer. Throughout this paper, the term TPE thus refers to Versaflex® CL30, although other commercially available thermoplastic elastomers would also be compatible with the fabrication techniques and fluidic operations described herein.

2.1. TPE membranes with open through-holes

We have developed a method that allows microscopic, high aspect-ratio open through-holes in a thin sheet of TPE to be produced in a reliable and efficient manner with virtually no modification to standard hot-embossing schemes.[57] This contrasts with the patterning of open through-holes in most hard thermoplastics for which sophisticated setups, alignment procedures, and post-processing steps are typically required.[58] As illustrated in Fig. 1a, a pre-extruded sheet of TPE is placed between a mold and a flat counter plate. The TPE sheet has a thickness that matches or slightly exceeds the height of the features on the mold. The stack is heated and exposed to elevated pressure until the features of the mold nearly reach the counter plate, typically leaving a thin residual TPE layer between them. When thin enough (e.g., <1 μm), the residual layer detaches from the membrane upon disassembly of the stack, thus giving rise to open through-hole features. We applied different surface treatments to both the mold and counter plate (see Section 5) to ensure that the TPE membrane remains adhering to the counter plate during the demolding process. The mold can thus be reused immediately for another embossing cycle, while the counter plate provides a carrier to facilitate the manipulation of the membranes in subsequent post-processing steps. As illustrated in Fig. 1a, this technique also permits the cutting of the membranes during the hot embossing step by placing a wall around each fluidic unit on the mold. Using a mold of 4″ in diameter, we were able to routinely pattern and precisely cut up to 32 open through-hole membranes of 1 × 1 cm^2 in a single step.

Fig. 1b shows a scanning electron microscopy (SEM) image of an array comprising square-shaped holes that are 30 μm in width and 90 μm in depth patterned in TPE using a silicon/SU-8 mold. The features are well defined and no residual TPE layer or deformation is apparent for the through-holes. By using a TPE sheet of appropriate thickness as starting material, we found that open through-holes can be obtained in less than 10 min embossing time by applying a force of 10 kN to the 4″ mold. Although shorter dwell times could be achieved at higher embossing forces, this relatively low force limits damage of the SU-8 features and permits a mold to be reused multiple times (thus eliminating the need for the preparation of costly metallic molds).

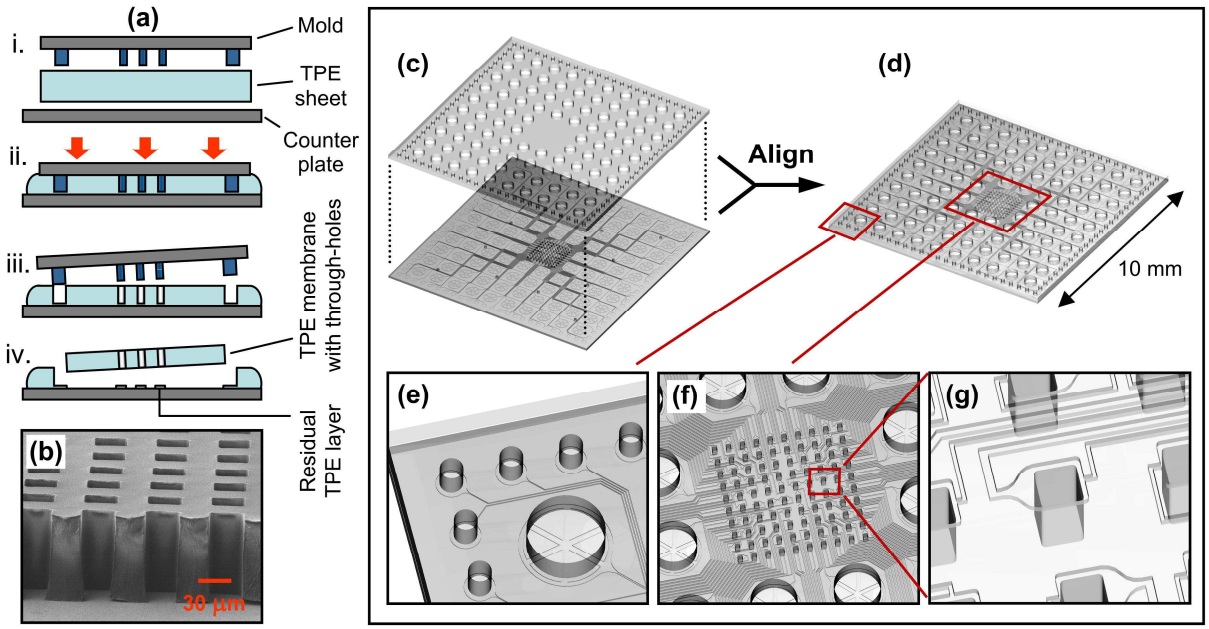

Fig. 1 (a) Schematics of the HEL process developed for the fabrication of TPE membranes with open through-holes. (b) SEM image (cross-sectional view) of a TPE membrane with open through-holes. (c)–(g) 3D CAD schematics showing the design of the microfluidic immobilization device developed in this work. (c)–(d) Both top and bottom membranes are aligned and placed in contact to form a 3D microfluidic system (see text for details). (e) Close-up view of the inlets and outlets of the device. (f) The central part comprises an array of spotting holes arranged in a 10 × 10 configuration. (g) Each spotting hole can be addressed individually through a set of incoming and outgoing supply channels.

The technique described herein shares similarities with the process developed for the fabrication of membranes with open through-holes in PDMS.[36,40,59] However, the use of thermoplastics rather than thermoset polymers such as PDMS presents several advantages for the fabrication and use of the membranes. For example, the starting material (i.e., either pellets or an extruded sheet of TPE) can be stored for extended periods of time and used on demand. Thermoset materials, on the other hand, require timely and elaborative preparation that involves mixing, degassing, and casting of liquid prepolymer components. These steps, combined with the time required for curing of the prepolymer complicate the use of thermosets in mass-production of microfluidic devices. The cost per kg of most TPEs is also considerably lower than that of PDMS, which would lead to very significant savings in a mass production process.[55] Moreover, thin membranes fabricated from standard PDMS formulations (e.g., Sylgard® 184) are relatively fragile, which makes their handling non-trivial and limits the scope of possible applications. The co-polymer structure of TPE can provide superior mechanical characteristics as reflected by the relatively large elongation at break (e.g., 780% for CL30 *vs.* ~140% for PDMS[60]), which minimizes the risk of damage during removal from the mold and thus provides better margins to scale both vertical and lateral dimensions of the features. Finally, if required, permanent bonding of two TPE membranes can be achieved conveniently by exposing them to elevated temperature after alignment.[53] For PDMS, O_2 plasma treatment needs to be performed immediately before aligning the membranes and pressing them together.[36,54]

2.2. Design of the 3D microfluidic immobilization device

The layout of the microfluidic immobilization device developed in this work is depicted in Figs. 1c–g. The device is based on two open through-hole membranes. The top membrane defines 96 inlets and 96 outlets while the bottom membrane is patterned with both a 10 × 10 array of 50 µm spotting holes in the centre part and a set of 96 independent supply channels that connect the spotting holes with the corresponding inlet and outlet reservoirs. The microfluidic device is thus designed as a fluidic concentrator which mediates the transport of liquid from macroscopic entry ports to micron-size regions defined by the spotting holes in the centre of the device. The dimensions of the devices are kept to 1 × 1 cm^2 in order to increase the production throughput and facilitate their integration with detection systems that have a relatively small footprint (e.g., a microfabricated biosensor chip).

As shown in Fig. 1f, a rather high density of channels is required to address each spotting hole independently, which imposes channel dimensions and inter-channel spacing in the range of 5 to 10 µm. Note that four of the 96 channels are connected to two spotting holes to compensate for the smaller number of inlets. To facilitate the manual filling of the devices, the 96 inlets are kept as large as possible (i.e., 500 µm in diameter) and dispersed evenly across the surface of the device, while the 96 outlets (150 µm in diameter) are distributed along the periphery of the device. The design has been optimized to drive the liquid through the channels by capillary action only, which represents a far more practical option than interfacing such a highly-integrated device with an external pumping system. The channel segment placed below each inlet has been patterned in a "star-shape" configuration (Fig. 1e) to ensure proper filling of the device by capillary action in the eventuality that the dispensed liquid is not distributed evenly in the inlet. The shape of the

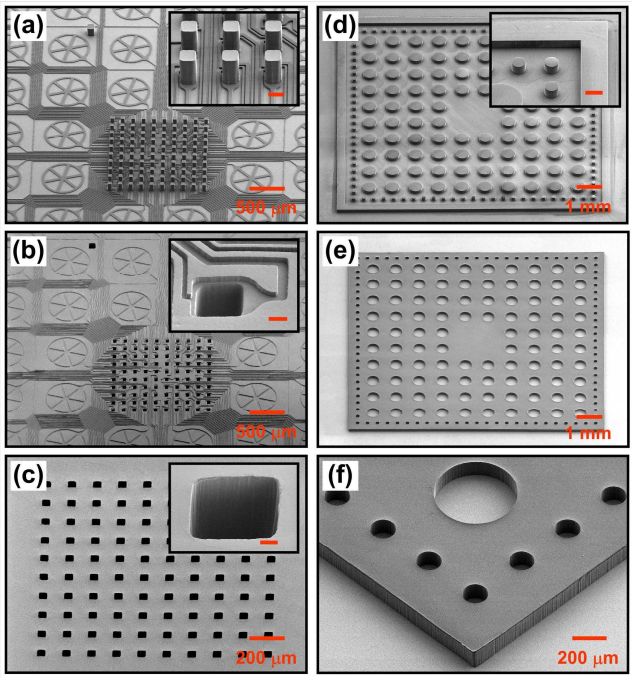

Fig. 2 SEM images illustrating the fabrication of the microfluidic device. (a) SU-8 embossing mold used for the fabrication of the bottom TPE membrane. (b) Upper and (c) lower side of the bottom TPE membrane. (d) SU-8 mold used for the fabrication of the top TPE membrane. (e) Overview and (f) close-up view of the top TPE membrane. Scale bars in the insets of (a), (b), (c) and (d) correspond to 50, 20, 10 and 200 µm, respectively. The images shown in (d) and (e) were assembled from several SEM micrographs to achieve the desired field of view.

channels around the spotting holes (Fig. 1g) has also been optimized to facilitate the filling of the holes by capillary action (see Section 3.2 for details).

In previous 3D microfluidic immobilization devices, isolated spots were typically obtained by transferring back and forth the liquid from channels embedded inside the device to channels in contact with the substrate via open through-holes.[36,38-41] This geometry implies that the area patterned on the substrate is larger than the through-holes, as two "vias" are required to create each isolated spot. The immobilization of biological probes on small areas thus depends on the fabrication of very small open through-holes, which is technically challenging. The practical realization of such a device also requires accurate alignment to properly register the two layers of channels, which is particularly difficult for elastomeric materials.[36] In this paper, we rather propose a design based on a single layer of channels where the biomolecules are immobilized directly by filling the open through-holes (Fig. 1g). With this layout, the accuracy required for alignment between the top and bottom membranes of the device is greatly relaxed as the registration between the channels and "vias" is performed directly during the fabrication of the mold (Fig. 2a). The tolerance for alignment between the two TPE membranes is ~70 µm while accuracy in the range of 5 to 10 µm would have otherwise been required with previous layouts. Also, with this new design, a spot size of 50 µm can be achieved without the need for punching open through-holes of smaller dimensions. Hence, the proposed layout greatly facilitates the fabrication and assembly of the device, which is important when production at low cost is being considered. On the other hand, a rather obvious disadvantage of the proposed design is the possibility to trap air bubbles above the spotting holes during the assays. We show in section 3.2 how this problem can be addressed by applying an appropriate design to the channel segment around the spotting holes.

2.3. Fabrication and assembly of the TPE membranes

Fig. 2a shows SEM micrographs of a silicon/SU-8 mold used for the fabrication of the bottom membrane. The mold consists of two SU-8 layers: an 8-µm-thick layer defines the channels and a 100-µm-thick layer patterned in a 10 ×10 array of pillars creates the open through-holes. Figs. 2b and 2c show images of the corresponding TPE membrane after hot embossing. Fig. 2b depicts the top side of the TPE membrane where both channels (that will be embedded inside the final device) and the top of the spotting holes are visible. Fig. 2c shows a TPE membrane that has been flipped to reveal the openings that will be in contact with the substrate during the immobilization process. Both channels and spotting holes were replicated very accurately. We found that the elastomeric nature of the TPE facilitates demolding and prevents the formation of defects resulting from undercut features, sidewall roughness, or shrinkage (which are commonly observed for HEL with hard thermoplastic substrates[58]). Fig. 2d shows one of the 32 units that we implemented on the silicon/SU-8 mold to pattern the top TPE membrane of the device. In addition to the pillars used to define inlets and outlets, the SU-8 wall surrounding each of the individual units is also visible. Figs. 2e and 2f show the corresponding open through-hole TPE membranes. These images highlight how the developed technique can be used not only to pattern microscopic "vias" and spotting holes, but also to punch a large number of inlets and outlets in a highly parallel manner and to effortlessly cut each of the individual membranes with very high accuracy.

After the patterning by HEL, the bottom and top TPE membranes were exposed to O_2 plasma to render their surface hydrophilic. This treatment was performed while the membranes were still attached to the hard counter plate, thus allowing numerous membranes to be treated simultaneously with a minimum of manipulation. Alignment of the top and bottom membranes was realized using an optical microscope equipped with an additional *x*-*y*-*z* translation stage that was placed on top of the movable sample platform. The top membrane was placed face-down on a transparent Teflon® sheet attached to the *x*-*y*-*z* manipulator, while the bottom membrane was placed on a substrate that was deposited on the microscope stage. When acceptable alignment was achieved, the manipulator was lowered until the two membranes were touching one another. Due to the rather weak adhesion force between TPE and Teflon®, the top membrane could be easily transferred and attached to the bottom membrane. No other bonding steps were necessary to operate the devices due to the watertight (yet reversible) sealing capability of TPE.

3. Fluidic operation and immobilization

3.1. General operation

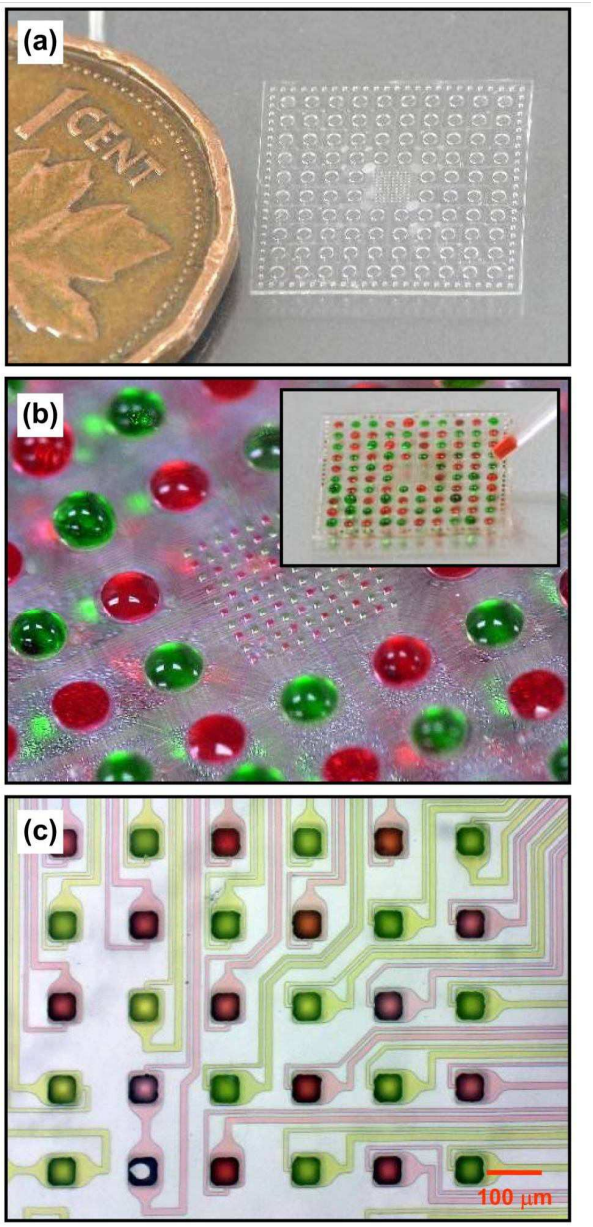

Fig. 3 Photographs of an assembled 3D microfluidic immobilization device (a) before and (b) after filling with solutions of a red and green dye. (c) Optical microscope image of the resulting red-green pattern obtained on the central region of the microfluidic device.

Fig. 3a shows an assembled 3D microfluidic immobilization device attached to a transparent plastic substrate. The device in Fig. 3b was charged entirely with two solutions containing either a red or green colored dye. Here, the dyes have been arranged in the form of a red-green chessboard pattern as revealed in Fig. 3c, thus demonstrating the possibility to address individually the spotting holes. Since the liquid tends to align itself on the cavities formed by the inlets, the dispensed droplets can be placed quite accurately on the surface of the devices despite the positional error introduced by manual pipetting (Fig. 3b). However, we found that it is relatively challenging to precisely control the amount of liquid dispensed at each position as the volume required to fill the inlets (e.g., ~50 nl) is outside the range of what can be accurately dispensed with most pipettes. We also noticed that, if the humidity of the ambient is not controlled properly, significant evaporation of the dispensed liquid takes place during the time (~15 min) required for filling the 96 inlets of the device. On the other hand, because the devices are filled by capillary action and have precisely positioned microfabricated inlets, they could be easily interfaced with automated, robotic-based dispensing systems to achieve better control over the volume dispensed and evaporation. Finally, due to the relatively high density of channels in this design, cleanliness of the environment during the assembly and monitoring of defects are important to prevent channel-to-channel leakage during fluidic operation.

3.2. Filling of the spotting holes by capillary action

The spotting holes need to be filled by capillary action without the trapping of air bubbles. This is particularly challenging as the deep wells formed by the spotting holes naturally act as capillary valves that block the liquid front. The layout of the channels has thus been designed and optimized with the help of 3D numerical simulations based on the Lattice-Boltzmann method.[60-62] Fig. 4a shows the various steps by which the liquid enters the spotting holes while Fig. 4b shows a Lattice-Boltzmann simulation for a channel with a similar geometry. The width of the channel has been increased from 10 to 60 μm just before the 50 μm spotting hole is reached. The larger width of the channel permits the liquid to surround the spotting hole, which reduces the radius of curvature of the liquid front in the plane of the device. This, in turn, increases the force exerted by the capillary action, which helps filling the spotting holes.[61] On the other hand, both simulations and experiments indicate that it takes considerably longer to fill the spotting holes than the surrounding channels. Consequently, air bubbles are trapped if the liquid in the surrounding channel is not held in place until the hole is properly filled. As shown in Figs. 4a and 4b, a sudden narrowing of the channel on the right-hand side of the hole ensures that the liquid cannot enter the exit channel before the hole is completely filled with liquid. The shape of the exit channel creates a capillary valve that stops the liquid on both sides while allowing air to be evacuated during the filling process. Figs. 4c and 4d illustrate how air bubbles are being trapped when the width of the channel is reduced gradually (rather than abruptly) after the spotting hole, preventing the liquid from entering the cavity. An example demonstrating this effect is shown on the bottom left corner of Fig. 3c. These results show that a careful design of the channels is required for proper filling of the spotting holes by capillary force. Without this optimization, about 30 min of incubation time is necessary before the air bubbles disappear and the holes are completely filled with liquid. A more detailed numerical analysis of the filling of 3D channels by capillary forces based on the Lattice-Boltzmann method is available elsewhere.[61]

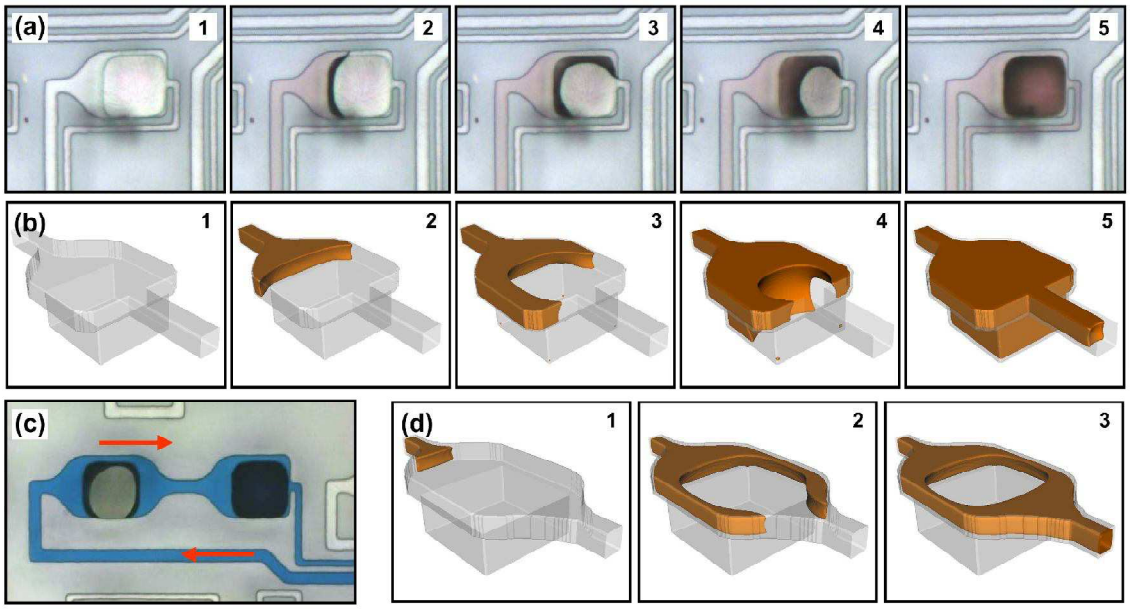

Fig. 4 (a) Sequence of optical micrographs and (b) Lattice-Boltzmann numerical simulations showing the filling process of the spotting holes by capillary forces. (c) Optical micrograph illustrating the effect of channel geometry on the trapping of air bubbles. (d) Lattice-Boltzmann numerical simulations using a channel design that leads to air bubbles being trapped above the spotting holes.

3.3. Immobilization of biological probes

Fig. 5 shows an example of a typical DNA immobilization assay in which a 3D microfluidic device has been used to pattern amino-modified Cy5-labeled DNA probes on an activated Zeonor substrate (see Section 5 for details). As shown in Fig. 5a, some of the channels have been filled selectively with the DNA solution to pattern the letters "IMI" while the other channels were left empty. Fig. 5b shows a fluorescence image of the Zeonor substrate after immobilization, removal of the microfluidic device, and washing. The 50 μm Cy5-labeled DNA spots corresponding to the spotting holes that have been filled during the assay are faithfully revealed. The edges of the spots are sharply defined and their relative positioning is controlled very accurately. Figs. 5c and 5d reveal that the uniformity of each spot is excellent, providing a root mean square (rms) variation in fluorescence intensity of only 2% on average. This result contrasts with the uniformity typically obtained by other techniques such as pin spotting, for which high spot uniformity is challenging to achieve at this scale.[1,22,23] As revealed by the example in Fig. 5b, spot-to-spot variation of fluorescence intensity was on the order of 20% rms when the same analyte was used to pattern each spot. We believe that this variation primarily arises from partial evaporation of the immobilization solution during the filling process and the difficulties in controlling precisely the volume dispensed in each inlet. Better control over the spot-to-spot uniformity could therefore be obtained by using an automated dispensing system placed in a humidy- and temperature-controlled environment. It is also noteworthy that no correlation was found between spot intensity and the length of the channel connecting the inlets to the spotting holes, indicating that absorption of DNA on TPE is small enough not to affect the immobilization process.

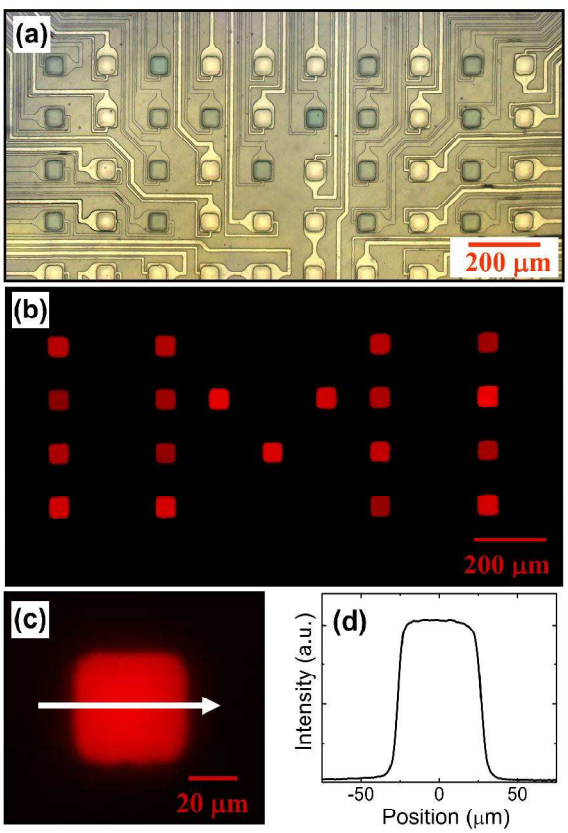

Fig. 5 Patterning of Cy5-labeled DNA probes on a Zeonor substrate using a 3D microfluidic immobilization device. (a) Optical microscope image showing a set of channels filled with the DNA solution. (b)–(c) Fluorescence microscope images of DNA spots on the Zeonor substrate. (d) Fluorescence intensity profile of the spot shown in (c).

An immobilization and hybridization assay performed with proteins is shown in Fig. 6. Here, solutions of unlabeled mouse and rabbit IgG (at a concentration of 5 mg/ml each) were dispensed in selected portions of the device according to

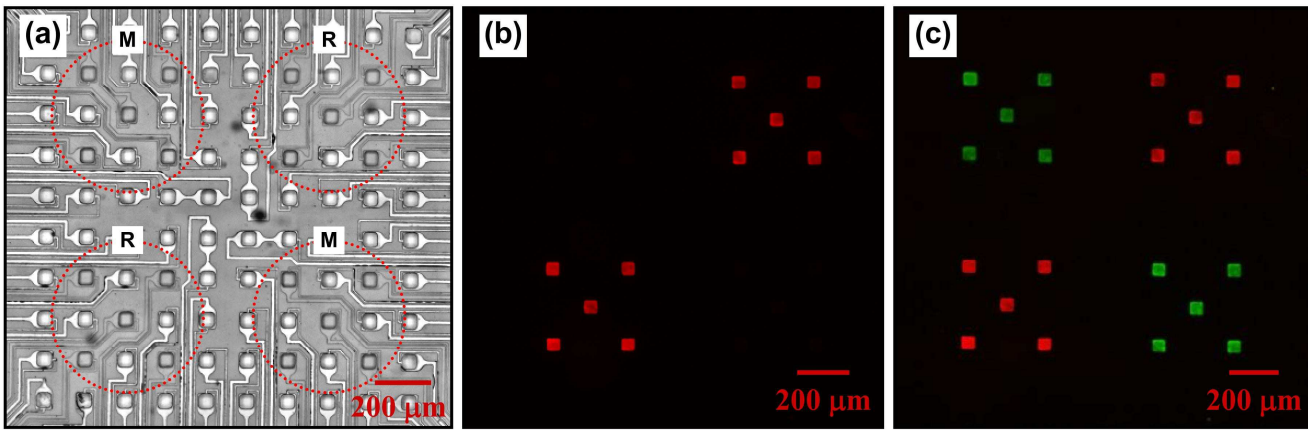

Fig. 6 Immobilization and hybridization of proteins on a Zeonor substrate. (a) Optical microscope image showing the channels filled with rabbit and mouse IgG solutions. The letters M and R indicate the respective segments of the array that were used for incubation with either mouse or rabbit IgG solution. (b) Fluorescence microscope images of the Zeonor substrate after hybridization with Cy5-labeled goat anti-rabbit IgG and (c) after subsequent hybridization with Cy3-labeled sheep anti-mouse IgG. Red and green colors denote the Cy5 and Cy3 channels of the fluorescence microscope.

the layout shown in Fig. 6a for the immobilization on an activated Zeonor substrate. As these biological probes were unlabeled in this assay, the Zeonor substrate showed no significant fluorescent signal after immobilization of the IgG proteins (data not shown). The substrate was sequentially exposed to Cy5-labeled goat anti-rabbit IgG (10 µg/ml) and Cy3-labeled sheep anti-mouse IgG (10 µg/ml). Fig. 6b shows the fluorescence signal recorded after hybridization with only the Cy5-labeled goat anti-rabbit IgG. As expected, a strong Cy5 fluorescence signal is recorded on the spots patterned with rabbit IgG. Relatively high hybridization selectivity was obtained: the measured Cy5 fluorescence intensity was ~150 times lower on the mouse IgG spots than on those modified with the complementary rabbit IgG. Fig. 6c shows a Cy3 (green) and Cy5 (red) combined fluorescence image obtained after subsequent hybridization of the Zeonor substrate with Cy3-labeled sheep anti-mouse IgG. Hybridization of the anti-mouse IgG was also highly selective with significant Cy3 fluorescent signal detected only on the mouse IgG spots. These results confirm the integrity of the immobilized protein array and show that the 3D microfluidic device can be used to immobilize high quality arrays.

4. Conclusions

We have developed a 3D microfluidic immobilization device using materials and techniques compatible with mass production. We demonstrated a technique based on HEL to pattern micron-size open through-holes in thin membranes made of commercially available TPE. The TPE membranes provided the basis for the fabrication of microfluidic devices capable of immobilizing up to 96 biological probes independently on a 10×10 array of isolated features that are 50 µm size. By using Lattice-Boltzmann numerical simulations, we proposed an optimized channel geometry that permits the use of capillary action to reliably fill the devices despite a complex 3D layout. Using these devices enables DNA and proteins to be immobilized with high spot uniformity and excellent positional accuracy.

Although the ultimate resolution achievable with these devices might not be competitive with that of scanning probe-based approaches,[62] they provide the interesting possibility to achieve high quality immobilization of custom probes on microfabricated biosensors in a point-of-care environment without the need for specialized equipment. Herein, we only presented examples of open-through membranes fabricated in a particular grade of TPE (Versaflex® CL30), hence the wide range of commercially available TPE materials could provide a key advantage to resolve some of the longstanding issues related to the integration of bioassays in microfluidics, including biocompatibility of materials, fouling, hydrophilization of surfaces, replication at low cost, and bonding, among others. We thus believe that the concepts emphasized within this paper provide a new toolset not only for the immobilization of biological probes at the micron-scale, but also for the high-throughput fabrication of advanced 3D microfluidic devices at low cost.

5. Materials and methods

Versaflex® CL30 (received in the form of pellets; GLS Corp., McHenry, IL) was extruded at a temperature of 165 °C to form sheets that are several meters long, ~15 cm wide and either ~140 or ~240 µm thick. Molds for HEL were prepared by photolithography using SU-8 photoresist (GM1060 and GM1075; Gersteltec, Pully, Switzerland) on a 4″ silicon wafer.[29] Photoplotted Mylar films printed at a resolution of 65,000 dpi (Fineline Imaging, Colorado Springs, CO) were used as photolithography masks. After the patterning of the SU-8 features, an anti-adhesive treatment was applied to the molds by spin-coating a thin layer of Teflon® AF (DuPont, Wilmington, DE) and post-annealing at 200 °C for 2 h. For the fabrication of the microfluidic devices, a piece of TPE was cut from the extruded sheet and placed between the mold and a counter plate. The counter plate consisted of a silicon wafer coated with either (i) 1*H*,1*H*,2*H*,2*H*-perfluoro-octyltrichlorosilane (Sigma-Aldrich, St. Louis, MO) deposited from the vapor phase under reduced pressure or (ii) a thin layer of PDMS (Sylgard 184; Dow Corning Corp., Midland, MI) deposited by spin-coating a degassed pre-polymer

mixture followed by curing at 200 °C for 2 h. HEL was performed using an EVG520 system (EV Group, Schärding, Austria) at a temperature of 170 °C, an applied force of 10 kN, and a pressure of 10^{-2} mbar. Oxygen plasma treatment (Plasmalabs 80plus; Oxford Instruments, Bristol, UK) was performed for 4 min at a pressure of 50 mTorr and an O_2 flow rate of 20 sccm. SEM images were acquired using a Hitachi S-4800 (Hitachi High-Technologies Canada, Mississauga, ON). Optical micrographs were taken with a Nikon Eclipse L150 microscope (Nikon Instruments, Melville, NY). The microfabrication steps and device assembly were carried out in a class 1000 clean room facility.

Numerical simulations were performed using a home-developed code based on the Lattice-Boltzmann method with a two-phase three-dimensional D3Q19 scheme driven by a Shan–Chen-type mesoscopic potential.[61,63,64] The contact angle of the liquid with the surface was set to a value of about 56° by adjusting the solid-liquid interaction potential. No external force was applied to the liquid. A more detailed description of the numerical simulations is available elsewhere.[61]

The protein and DNA immobilization assays were performed on plastic substrates (25 mm in width, 75 mm in length and 1 mm in height) that were fabricated from Zeonor 1060R (Zeon Chemicals, Louisville, KY) by an injection molding process. Before the immobilization assays, the Zeonor slides were subjected to an ozone treatment for ~15 min using an Ozo 2vtt ozone generator (Ozomax, Shefford, QC). They were then incubated with a freshly prepared solution of 17 μM *N*-hydroxysuccinimide (NHS; Sigma-Aldrich) and 42 μM 1-ethyl-3-[3-dimethyl-aminopropyl]carbodiimide hydrochloride (EDC; Sigma-Aldrich) in phosphate buffered saline (PBS, pH 7.4; Sigma-Aldrich) for 90 min,[65] rinsed with de-ionized (DI) water and dried with a stream of nitrogen gas. Amino-modified 27-mer oligonucleotides labeled with a Cy3 or Cy5 fluorophore (Integrated DNA Technologies, Coralville, IA) were dissolved in DI water to obtain a 40 μM solution, which was diluted 1:1 (v/v) with dimethyl sulfoxide (Sigma-Aldrich) for the DNA immobilization assays. Proteins were purchased from Jackson ImmunoResearch Laboratories (West Grove, PA) and diluted in PBS.

To perform immobilization, a 3D microfluidic device was placed on a freshly activated Zeonor slide. The inlets were each filled with ~50 nL of solution using a micropipette. After 2 h of incubation in a humid environment at room-temperature, the Zeonor substrate was immerged in a solution of 0.1% sodium dodecyl sulfate (SDS; Sigma-Aldrich) in PBS and the microfluidic device was peeled off the surface. The Zeonor substrate was then washed with 0.1% SDS in PBS for 5 min and rinsed with DI water. Each microfluidic device was used only once to avoid cross-contamination issues. Before hybridization, the Zeonor substrate was blocked using a solution of 1 mg/ml bovine serum albumin (BSA; Sigma-Aldrich) in PBS for 15 min at room-temperature. Hybridization of proteins was done in a passive manner by spreading 10 μl of the target solution on top of the Zeonor substrate using a glass cover slip. After 30 min of incubation, the cover slip was removed and the Zeonor substrate was rinsed with PBS and DI water. Fluorescence imaging was done using an Eclipse TE2000-U inverted fluorescence microscope (Nikon Instruments) equipped with an EM-CCD camera (Hamamatsu, Bridgewater, NJ).

Acknowledgements

This work was supported by the National Research Council's Genomics and Health Initiative Program and the Industrial Materials Institute. We thank the Réseau québécois de calcul de haute performance (RQCHP) for providing the computational resources for the numerical simulations. We are grateful to our colleagues Gerardo A. Diaz-Quijada, Hélène Roberge and Kien-Mun Lau for useful discussion and technical assistance. John Pezacki from the National Research Council's Steacie Institute for Molecular Sciences is acknowledged for his strong support of this work.

References

1. I. Barbulovic-Nad, M. Lucente, Y. Sun, M. Zhang, A. R. Wheeler and M. Bussmann, *Crit. Rev. Biotechnol.*, 2006, **26**, 237-259.
2. K.-Y. Tomizaki, K. Usui and H. Mihara, *ChemBioChem*, 2005, **6**, 782-799.
3. S. C. Lin, F. G. Tseng, H. M. Huang, C. Y. Huang and C. C. Chieng, *Fresenius. J. Anal. Chem.*, 2001, **371**, 202-208.
4. C. Debouck and P. N. Goodfellow, *Nat. Genet.*, 1999, **21**, 48-50.
5. R. Peytavi, F. R. Raymond, D. Gagné, F. J. Picard, G. Jia, J. Zoval, M. Madou, K. Boissinot, M. Boissinot, L. Bissonnette, M. Ouellette and M. G. Bergeron, *Clin. Chem.*, 2005, **51**, 1836-1844.
6. D. J. Lockhart and E. A. Winzeler, *Nature*, 2000, **405**, 827-836.
7. W. J. Ansorge, *New Biotechnol*, 2009, **25**, 195-203.
8. F. Teles and L. Fonseca, *Talanta*, 2008, **77**, 606-623.
9. G. Zheng, F. Patolsky, Y. Cui, W. U. Wang and C. M. Lieber, *Nat. Biotechnol.*, 2005, **23**, 1294-1301.
10. E. Stern, J. F. Klemic, D. A. Routenberg, P. N. Wyrembak, D. B. Turner-Evans, A. D. Hamilton, D. A. LaVan, T. M. Fahmy and M. A. Reed, *Nature*, 2007, **445**, 519-522.
11. E. Stern, A. Vacic, N. K. Rajan, J. M. Criscione, J. Park, B. R. Ilic, D. J. Mooney, M. A. Reed and T. M. Fahmy, *Nat. Nanotechnol.*, 2010, **5**, 138-142.
12. B. Y. Lee, S. M. Seo, D. J. Lee, M. Lee, J. Lee, J.-H. Cheon, E. Cho, H. Lee, I.-Y. Chung, Y. J. Park, S. Kim and S. Hong, *Lab Chip*, 2010, **10**, 894-898.
13. A. Kim, C. S. Ah, H. Y. Yu, J.-H. Yang, I.-B. Baek, C.-G. Ahn, C. W. Park, M. S. Jun and S. Lee, *Appl. Phys. Lett.*, 2007, **91**, 103901.
14. C. H. Kim, C. Jung, H. G. Park and Y. K. Choi, *Biochip J.*, 2008, **2**, 127-134.
15. A. Densmore, M. Vachon, D.-X. Xu, S. Janz, R. Ma, Y.-H. Li, G. Lopinski, A. Delâge, J. Lapointe, C. C. Luebbert, Q. Y. Liu, P. Cheben and J. H. Schmid, *Opt. Lett.*, 2009, **34**, 3598-3600.
16. C. F. Carlborg, K. B. Gylfason, A. Kaźmierczak, F. Dortou, M. J. Bañuls Polo, A. Maquieira Catala, G. M. Kresbach, H. Sohlström, T. Moh, L. Vivien, J. Popplewell, G. Ronan, C. A. Barrios, G. Stemme and W. van Der Wijngaart, *Lab Chip*, 2010, **10**, 281-290.
17. A. Prabhakar and S. Mukherji, *Lab Chip*, 2010, **10**, 748-754.

18. O. Hofmann, G. Voirin, P. Niedermann and A. Manz, *Anal. Chem.*, 2002, **74**, 5243-5250.
19. J. M. Goddard, S. Mandal, S. R. Nugen, A. J. Baeumner and D. Erickson, *Colloids Surf., B*, 2009, **76**, 375-380.
20. L. Soleymani, Z. Fang, S. O. Kelley and E. H. Sargent, *Appl. Phys. Lett.*, 2009, **95**, 143701.
21. M. Schena, D. Shalon, R. W. Davis and P. O. Brown, *Science*, 1995, **270**, 467–470.
22. J. T. Smith, B. L. Viglianti and W. M. Reichert, *Langmuir*, 2002, **18**, 6289-6293.
23. M. K. McQuain, K. Seale, J. Peek, S. Levy and F. R. Haselton, *Anal. Biochem.*, 2003, **320**, 281-291.
24. A. Pierik, F. Dijksman, A. Raaijmakers, T. Wismans and H. Stapert, *Biotechnol. J.*, 2008, **3**, 1581-1590.
25. T. Okamoto, T. Suzuki and N. Yamamoto, *Nat. Biotechnol.*, 2000, **18**, 438-441.
26. E. Delamarche, *Microcontact Printing of Proteins*. In: *Nanobiotechnology: Concepts, Applications and Perspectives*, C. M. Niemeyer and C. A. Mirkin (eds), Wiley-VCH, Weinheim, Germany, 2005, 31-52.
27. R. S. Kane, S. Takayama, E. Ostuni, D. E. Ingber and G. M. Whitesides, *Biomaterials*, 1999, **20**, 2363-2376.
28. M. Geissler, E. Roy, J.-S. Deneault, M. Arbour, G. A. Diaz-Quijada, A. Nantel and T. Veres, *Small*, 2009, **5**, 2514-2518.
29. M. Geissler, E. Roy, G. A. Diaz-Quijada, J.-C. Galas and T. Veres, *ACS Appl. Mater. Interfaces*, 2009, **1**, 1387-1395.
30. D. B. Weibel, W. R. Diluzio and G. M. Whitesides, *Nat. Rev. Microbiol.*, 2007, **5**, 209-218.
31. E. Delamarche, A. Bernard, H. Schmid, B. Michel and H. Biebuyck, *Science*, 1997, **276**, 779-781.
32. E. Delamarche, A. Bernard, H. Schmid, A. Bietsch, B. Michel and H. Biebuyck, *J. Am. Chem. Soc.*, 1998, **120**, 500-508.
33. S. Takayama, J. C. McDonald, E. Ostuni, M. N. Liang, P. J. Kenis, R. F. Ismagilov and G. M. Whitesides, *Proc. Natl. Acad. Sci. U. S. A.*, 1999, **96**, 5545-5548.
34. A. Bernard, B. Michel and E. Delamarche, *Anal. Chem.*, 2001, **73**, 8-12.
35. H. Chen, L. Wang and P. C. H. Li, *Lab Chip*, 2008, **8**, 826-829.
36. D. T. Chiu, N. L. Jeon, S. Huang, R. S. Kane, C. J. Wargo, I. S. Choi, D. E. Ingber and G. M. Whitesides, *Proc. Natl. Acad. Sci. U. S. A.*, 2000, **97**, 2408-2413.
37. L. Griscom, P. Degenaar, B. LePioufle, E. Tamiya and H. Fujita, *Jpn. J. Appl. Phys.*, 2001, **40**, 5485-5490.
38. D. Juncker, H. Schmid, U. Drechsler, H. Wolf, M. Wolf, B. Michel, N. de Rooij and E. Delamarche, *Anal. Chem.*, 2002, **74**, 6139-6144.
39. D. Juncker, H. Schmid and E. Delamarche, *Nat. Mater.*, 2005, **4**, 622-628.
40. U. Kloter, H. Schmid, H. Wolf, B. Michel and D. Juncker, in *Technical Digest of the 17th IEEE International Conference on Micro Electro Mechanical Systems*, 2004, pp. 745-748.
41. Z.-H. Wang, Y.-H. Meng, P.-Q. Ying, C. Qi and G. Jin, *Electrophoresis*, 2006, **27**, 4078-4085.
42. D. A. Chang-Yen, D. G. Myszka and B. K. Gale, *J. Microelectromech. Syst.*, 2006, **15**, 1145-1151.
43. M. A. Eddings, A. R. Miles, J. W. Eckman, J. Kim, R. L. Rich, B. K. Gale and D. G. Myszka, *Anal. Biochem.*, 2008, **382**, 55-59.
44. S. Natarajan, A. Hatch, D. G. Myszka and B. K. Gale, *Anal. Chem.*, 2008, **80**, 8561-8567.
45. S. Natarajan, P. S. Katsamba, A. Miles, J. Eckman, G. A. Papalia, R. L. Rich, B. K. Gale and D. G. Myszka, *Anal. Biochem.*, 2008, **373**, 141-146.
46. M. A. Eddings, J. W. Eckman, C. A. Arana, G. A. Papalia, J. E. Connolly, B. K. Gale and D. G. Myszka, *Anal. Biochem.*, 2009, **385**, 309-313.
47. S. A. Vanapalli, D. Wijnperle, A. van Den Berg, F. Mugele and M. H. G. Duits, *Lab Chip*, 2009, **9**, 1461-1467.
48. J. A. Benn, J. Hu, B. J. Hogan, R. C. Fry, L. D. Samson and T. Thorsen, *Anal. Biochem.*, 2006, **348**, 284-293.
49. K. A. Fosser and R. G. Nuzzo, *Anal. Chem.*, 2003, **75**, 5775-5782.
50. R. Mukhopadhyay, *Anal. Chem.*, 2007, **79**, 3248-3253.
51. H. Becker, *Lab Chip*, 2009, **9**, 2759-2762.
52. H. Becker, *Lab Chip*, 2010, **10**, 271-273.
53. E. Roy, M. Geissler, J.-C. Galas and T. Veres, *Microfluid Nanofluid*, 2011, **11**, 235-244.
54. D. C. Duffy, J. C. McDonald, O. J. A. Schueller and G. M. Whitesides, *Anal. Chem.*, 1998, **70**, 4974-4984.
55. E. Roy, J.-C. Galas and T. Veres, *Lab Chip*, 2011, **11**, 3193-3196.
56. E. Roy, M. Mounier, R. Peytavi, J. Siegrist, R. Gorkin, M. Madou, M. G. Bergeron and T. Veres, in *Proceedings of the 14th International conference on miniaturized systems for chemistry and life sciences*, Groningen, 2010, pp. 1898–1901.
57. D. Brassard, K. Li, E. Roy and T. Veres, *PCT Patent application*, PCT/CA2011/000154, 2011.
58. M. Worgull, *Hot Embossing - Theory and Technology of Microreplication*, William Andrew, 2009.
59. B.-H. Jo, L. M. Van Lerberghe, K. M. Motsegood and D. J. Beebe, *J. Microelectromech. Syst.*, 2000, **9**, 76-81.
60. M. Liu, J. Sun, Y. Sun, C. Bock and Q. Chen, *Journal of Micromechanics and Microengineering*, 2009, **19**, 035028.
61. L. Clime, D. Brassard and T. Veres, *Accepted for publication in Microfluid. Nanofluidic.*, 2011.
62. L. M. Demers, D. S. Ginger, S.-J. Park, Z. Li, S.-W. Chung and C. A. Mirkin, *Science*, 2002, **296**, 1836-1838.
63. S. Chen and G. D. Doolen, *Annu. Rev. Fluid. Mech.*, 1998, **30**, 329-364.
64. L. Clime, D. Brassard and T. Veres, *Microfluid. Nanofluid.*, 2009, **8**, 599-608.
65. G. A. Diaz-Quijada, R. Peytavi, A. Nantel, E. Roy, M. G. Bergeron, M. M. Dumoulin and T. Veres, *Lab Chip*, 2007, **7**, 856-862.